Ultra-fast sintered functionally graded Fe/W composites for the first wall of future fusion reactors

S. Heuer[a,*], T. Lienig[a], A. Mohr[b], Th. Weber[a], G. Pintsuk[a], J.W. Coenen[a], F. Gormann[a], W. Theisen[b], Ch. Linsmeier[a]

[a] *Forschungszentrum Jülich GmbH, Institut für Energie- und Klimaforschung - Plasmaphysik, Partner of the Trilateral Euregio Cluster (TEC), 52425 Jülich, Germany*

[b] *Lehrstuhl Werkstofftechnik, Ruhr-Universität Bochum, 44780 Bochum, Germany*

Abstract

Aiming at the realisation of nuclear fusion reactors, the joining of W and steel parts is currently examined. Based on proposals to implement functionally graded steel/W materials (FGMs) in the joint to cope with thermal stresses, the present contribution introduces a novel fabrication method for steel/W FGMs. Electro Discharge Sintering (EDS) was used to consolidate Fe/W powders within milliseconds at atmosphere. Due to the short process time, the formation of detrimental intermetallic Fe-W precipitates is limited compared to established fabrication methods.

The current work first presents results of the Fe/W powder processing, then a feasibility study regarding the fabrication of homogeneous and graded Fe/W composites with W volume fractions of 0, 25, 50 and 75 % via EDS is presented. Lastly, the composites are characterised microstructurally, thermo-physically, and mechanically in detail.

Keywords:
Field-Assisted Sintering Technique (FAST), Electro Discharge Sintering (EDS), Functionally Graded Materials (FGMs), Metal Matrix Composites (MMC), Fe/W

1. Introduction

According to current understanding, future fusion reactors will feature W as the plasma facing material [1, 2]. At the first wall, W will be joined to a blanket structure made of reduced activation ferritic martensitic (RAFM) steel, e.g. Eurofer. Finite element analyses (FEA), applied for different geometries and reactor heat loads, have shown that intense stresses develop at a macroscopically discrete Eurofer-W joint during production and reactor operation that ultimately result in delamination of the W armour [3–7]. In order to avoid a macroscopically discrete transition of material properties at the Eurofer-W interface, functionally graded steel/W materials are being developed [8–10]. Functionally graded materials (FGMs) approximate the adjacent materials' properties by gradually varying the constituents composition over the FGM's height and represent one viable option of interlayer systems to cope with thermal stresses and plastic deformation in the first wall of fusion reactors. Other potential interlayer systems are suggested in several publications [8, 11–26]. According to numerical calculations, FGMs for the first wall of DEMO will have to be at least 0.7 mm thick and contain three or more sublayers with differing constituent ratios [7]. Given this, thin film production methods, e.g. physical vapour deposition [8], and electro-chemical deposition [27, 28] are impracticable, whereas powder-metallurgical routes are more realistic. Among these, atmospheric and vacuum plasma spraying [8, 29], and resistive sintering under ultra-high pressure [10, 30] are promising and were already carried out for steel/W FGM production. All of the fabrication routes, however, have issues with the formation of cracks or intermetallic phases (Fe_7W_6, Fe_2W) due to extended exposure of the materials to high temperatures during production.

Electro discharge sintering (EDS) is a novel technique [31] that was first used for the fabrication of Fe/W composites in the context of the current work. EDS combines characteristics of spark plasma sintering (SPS) and capacitor discharge welding. The used facility is shown in Fig. 1. Similar to SPS, for EDS, powder is filled into a ring-shaped die. An electric current is

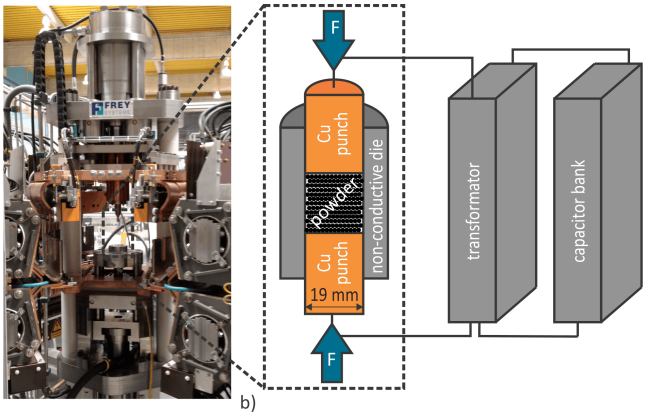

Figure 1: Facility for electro discharge sintering. a) Photography, b) sketch of the work principle.

*Corresponding author
Email address: s.heuer@fz-juelich.de (S. Heuer)

guided through the powder via vertical punches that additionally apply mechanical pressure to the powder. Due to uniaxial pressure and dissipation of electricity into heat, the powder is consolidated. In contrast to SPS, the EDS die is made of a non-conductive ceramic. Using this set up, it is ensured that the entire electric current is guided through the powder. Furthermore, Cu alloy punches are used for EDS, enabling higher mechanical pressures (up to 388 MPa) compared to conventional SPS with graphite punches. Similar to capacitor discharge welding, the EDS facility is equipped with a capacitor bank, which stores up to 80 kJ electrical energy. A single electric pulse of up to 400 kA at 50 V is generated, heating the powder. The combination of a short, high current and high uniaxial pressure consolidates the powder within milliseconds, making the need for controlled atmospheric conditions redundant. For the reason of thermodynamic simplicity, at this stage, only Fe/W FGMs were engineered instead of steel/W FGMs, and showed promising material properties.

2. Fabrication

Fabrication took place in two steps. First, homogeneous composites of several Fe/W volume ratios were consolidated. Then, actual FGMs were made by successively filling powders of different Fe/W volume ratios into the die of the EDS facility and consolidating the stacked mix in one discharge. Both homogeneous and graded samples were 19 mm in diameter and 3 mm high after consolidation. For both types of samples, initial powder processing was applied as follows.

2.1. Powder processing

Commercially available Fe and W raw powders of different particle sizes, listed in tab. 1 along with the corresponding oxygen contents, were used in the current work. The list contains two Fe and two W powders. Fe_{6-8} and W_{11-13} are referred to as "fine" and Fe_{20-40} and $W_{<25}$ as "coarse" powders. For powder mixing, the two fine raw powders and the two coarse raw powders were merged.

Table 1: Overview of utilised powders in the current work.

powder notation	supplier	nominal particle size class (μm)	O content[1] (wt.%)
Fe_{20-40}	Goodfellow	20-40 (after sieving from < 60 μm powder)	0.100±0.001
Fe_{6-8}	Goodfellow	6-8	0.294±0.005
$W_{<25}$	Goodfellow	<25	0.048±0.001
W_{11-13}	Eurotungstène	11-13	0.040±0.001

[1] measured by He carrier gas hot extraction

The powder morphologies are shown in Fig. 2. All raw powders consist of compact particles. While the smaller Fe_{6-8} particles are spherically shaped and contain some satellites, the larger Fe_{20-40} particles are irregularly shaped. Both Fe powders show smooth particle surfaces, which are characteristic of the applied production route, gas atomization. In contrast, the W particles are of polyhedral shape, being characteristic of electrolytic deposition. The reason for the high number of agglomerates of the smaller W_{11-13} particles is unclear. Agglomerates may relate to the deposition process or to a high electrical potential due to a great particle surface/volume ratio. All powders contain few particles that exceed the nominal particle size class.

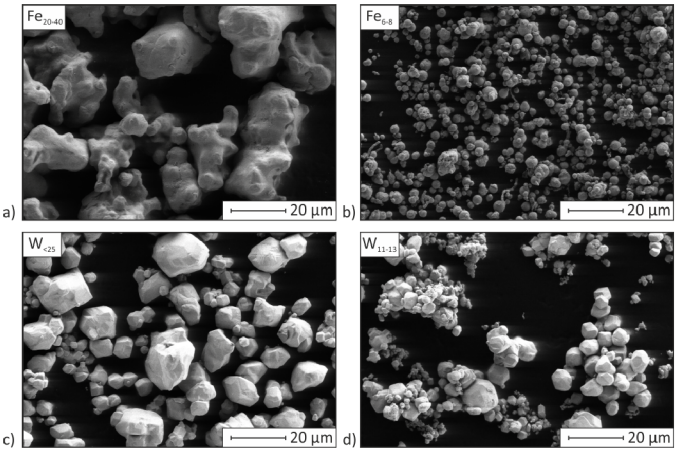

Figure 2: SEM images of the utilized raw powders a) Fe powder 20-40 μm, b) Fe powder 6-8 μm, c) W powder < 25 μm, d) W powder 11-13 μm.

For generating Fe/W powder mixtures, the raw powders were weighed at the W volume fractions 0, 25, 50 and 75 % using a precision balance. Coarse powders, Fe_{20-40} and $W_{<25}$, of the named W fractions were manually mixed for 5 min without external energy input. Fine powders, Fe_{6-8} and W_{11-13}, were energetically mixed using a planetary mill. Energetic mixing of the fine powders was necessary because powders consisting of particles < 10 μ m cannot be used in the EDS facility as particles may penetrate the gap between die and lower punch. The goal of energetic mixing was to create larger particles while retaining pure, finely distributed Fe and W volumes in each particle. The process is also referred to here as "incomplete mechanical alloying": In an Ar-filled glove box, a 125 ml, WC-coated mixing jar was filled with 40 g powder mixture, together with 200 g WC balls (∅ 5 mm) and then sealed to keep the Ar atmosphere. No additive was used. Exploration of suitable mixing durations was carried out mixing a 50 vol.% W containing powder mixture for 2, 4 and 8 hours at 200 rpm. Shorter mixing durations and lower rotation speed were found to result in no noticeable mixing and are not presented in detail.

2.2. Powder consolidation via EDS

Consolidation of manually mixed coarse powders and energetically mixed fine powders was carried out by applying EDS. Since an Fe/W FGM will be part of the first wall it must ensure high heat removal capabilities and maintain structural integrity. Pores and impurity phases may prevent achievement of these requirements by reducing thermal conductivity and increasing mechanical flaws. Hence, the goal of the current study was to identify a parameter set, suitable for generating dense

composites without intermetallics. Given this, besides differing raw powders and Fe/W ratios, uniaxial mechanical pressure and discharge energy of the EDS facility were varied in the current work. Selected pressures and discharge energies were 282 and 388 MPa, and 72 kJ and 80 kJ (90 and 100 % of the maximum discharge energy of the EDS facility), respectively.

After weighing and filling in the amount of powder mixture required for a dense, 19 x 3 mm^3 (∅ x h) sample, the upper punch is lowered onto the powder mix. The uniaxial pressure is raised until reaching the desired pressure. Next, the capacitor bank is discharged and the powder consolidated. Finally, the upper punch is brought back into its initial position and the compact composite is removed. Homogeneous and graded composites are fabricated following the same procedure. It may be noted here that measurement of the temperature during consolidation is inaccessible due to the short process time, the strong electric current, an inhomogeneous temperature field, and a closed design of the die.

3. Results and discussion

Evaluation of the EDS-based FGM fabrication feasibility and characterisation of the composites was done with respect to application of FGMs in the first wall of fusion reactors. Besides microstructural analysis, chemical, thermo-physical, and mechanical properties are of interest.

3.1. Fe/W Powders

Fe/W powders were mixed using coarse (Fe_{20-40} and $W_{<25}$) and fine (Fe_{6-8} and W_{11-13}) powders. Since mixing of the coarse powders occurred manually without input of energy, no morphological and chemical changes compared to the individual raw powders are to be expected. Detailed characterisation of powders is therefore limited here to the energetically mixed fine powders. Fig. 3 depicts SEM images of powders that were made from fine powders mixed for 2, 4 and 8 hours. All pictured powders contain 50 vol.% W.

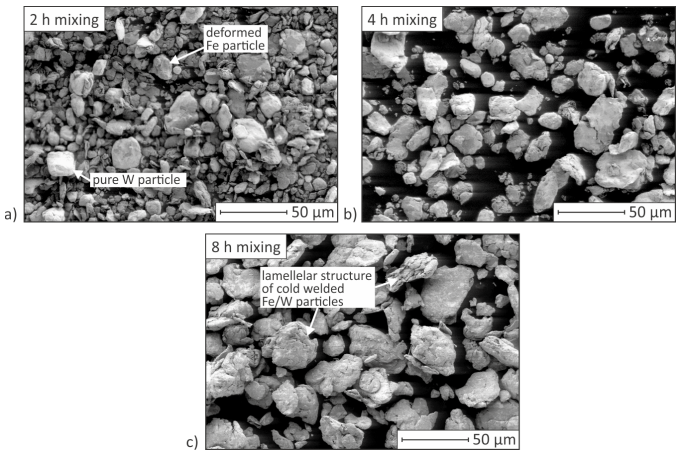

Figure 3: SEM images of Fe/W powders containing 50 vol.% W, energetically mixed in a planetary mill for different durations. Mixing occurred for a) 2 h, b) 4 h, c) 8 h.

Deep grey volumes indicate Fe, brighter grey volumes are W. With increasing mixing duration, the contrast is reduced. Along with that, the average particle size increases and saturates at 20-40 μm. Both observations base on cyclic plastification, hardening, cracking and cold (re-)welding [32]. For the given W fraction and mixing parameters, only after 8 hours mixing, no individual Fe or W particles can be observed, indicating 8 hours mixing is a reasonable processing time. Cross sections of powders containing 25, 50 and 75 vol.% W, mixed for this duration, are displayed in Fig. 4.

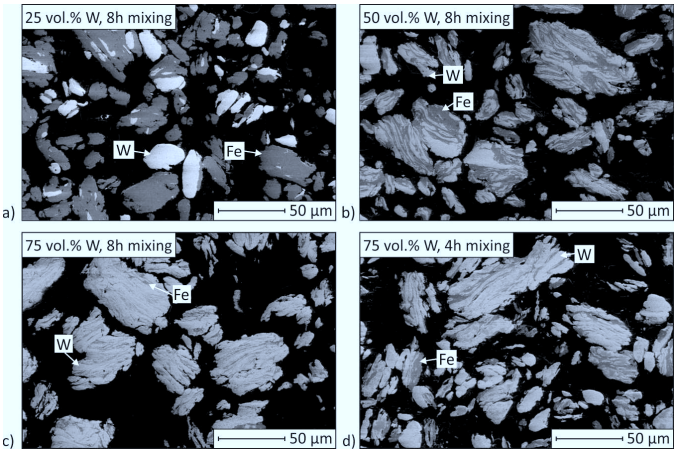

Figure 4: SEM cross sections of incompletely mechanically alloyed Fe/W powders of differing W vol.% fractions. a) 25 vol.% W (8 h mixing), b) 50 vol.% W (8 h mixing), c) 75 vol.% W (8 h mixing) d) 75 vol.% W (4 h mixing).

In Fig. 4 b), the Fe/W powder that was used for the described mixing duration study is again shown. The cross section confirms finely and homogeneously distributed constituents within the particles. Lamellar Fe and W volumes are related to cold welding upon collisions and indicate ductile behaviour of the constituents during mixing. The Fe/W distribution of powders containing 25 vol.% W (Fig. 4 a)) or 75 vol.% W (Fig. 4 c)), mixed with the same parameters, deviates from the morphology of the 50 vol.% W powder. It is assumed here that the miscibility is limited with greater Fe contents because Fe is softer and more ductile than W. With higher Fe fractions the probability of a soft Fe particle participating in a collision increases. The impulse is then transferred via a harder particle (W, previously hardened Fe or Fe/W) to the soft Fe particle, in which the collision energy is dissipated by plastic deformation. Consequently, cold welding is suppressed. In contrast, powders that contain smaller Fe fractions re-weld and mix very well. The powder containing 75 vol.% W, mixed for 8 hours, shows very thin lamellae. Very thin lamellae may in fact be detrimental here, as these are accompanied by high residual stresses and many constituent interfaces. This lowers the thermal conductivity and increases interdiffusion, promoting precipitation of intermetallics. Another Fe/W powder containing 75 vol.% W was thus mixed for 4 hours only. The cross section, exhibiting thicker lamellae compared to the respective powder mixed for 8 hours, is shown in Fig. 4 d).

For the prepared powders, X-ray diffraction (XRD) was carried out to determine whether the formation of intermetallics

could be suppressed by limiting the time of incomplete mechanical alloying. The diffractograms of representative powder

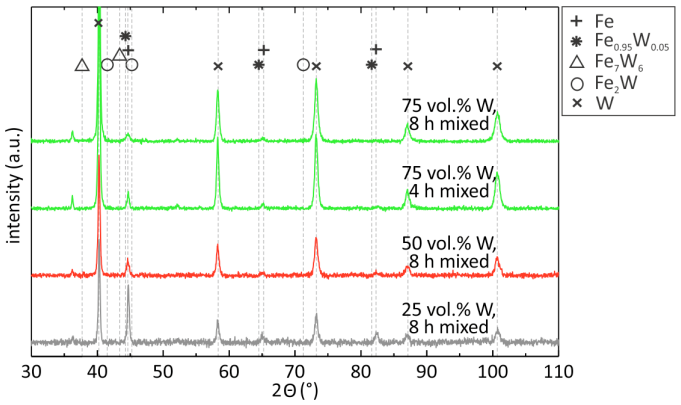

Figure 5: Diffractograms of powders mixed by incomplete mechanical alloying.

volumes are shown in Fig. 5. Theoretically expected diffraction peaks are indicated by individual symbols and dashed lines. Neither intermetallic precipitates, Fe_7W_6 or Fe_2W, nor the solid solution, $Fe_{0.95}W_{0.05}$, were detected. They either do not exist or volumes are too small for verification.

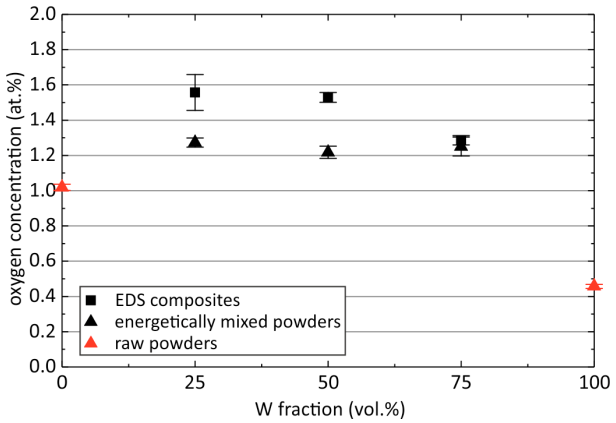

Figure 6: Oxygen content of raw powders, energetically mixed powders and consolidated Fe/W composites.

The oxygen content of all powders after mixing is given in Fig. 6 along with the oxygen content of the raw materials and the O content after sintering, measured by carrier gas hot extraction. The values indicate that oxidation during mixing is limited, compared to the natural O contamination of the Fe (1 at.%) and W powders (0.45 at.%).

3.2. *Fe/W Composites*

Composites were manufactured using the pure and mixed coarse powders, and the mixed fine powders. A macroscopic image of an exemplary composite is shown in Fig. 7. The surface is even but microscopically rough owing to a less effective consolidation of the upper- and lowermost 300 μm of each sample. Prior to characterisation, these volumes were removed by grinding. Consolidation of pure W powder was unsuccessful with any EDS parameter, probably owing to high electrical and thermal conductivity, combined with high strength. Hence, pure W samples are not characterised here.

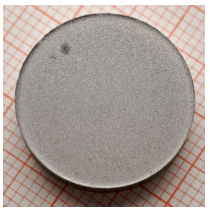

Figure 7: Exemplary macroscopic image of an EDS sample containing 50 vol.% W after consolidation.

3.2.1. *Composites from manually mixed coarse powders*

Composites made from manually mixed coarse powders were manufactured as homogeneous samples only. For aforementioned reasons, low residual porosity of all composites is required. Fig. 8 depicts the residual porosity of homogeneous samples made from coarse powders as a function of the W volume fraction. Two different discharge energies (72 kJ and 80 kJ) at 388 MPa uniaxial pressure were applied for EDS. The porosity was calculated via quantitative image analysis and Archimedes principle.

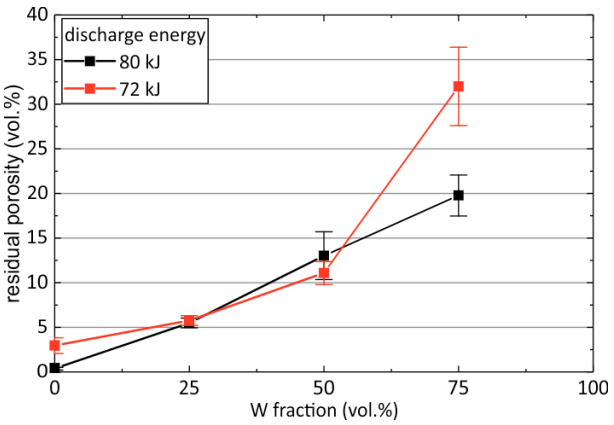

Figure 8: Residual porosity of composites made from manually mixed coarse Fe/W powders according to quantitative image analysis. The uniaxial pressure was set to 388 MPa, the discharge energies to 72 and 80 kJ (90 and 100 %).

While pure Fe powders reach theoretical density with 80 kJ discharge energy, increasing the W fraction or lowering the discharge energy causes higher porosity. The latter is particularly pronounced for composites of high W fractions and may well be explained by the general consolidation mechanism of EDS: Using EDS, powders are heated heterogeneously. Due to increased ohmic resistance, powder particle contact zones reach higher temperatures compared to particle volumes. Within contact zones diffusion is initiated, particles soften and may partially melt. Uniaxial pressure then compresses the powder to a solid component [31]. Although the heat capacity of W is only a third of the heat capacity of Fe (138 vs. 449 $Jkg^{-1}K^{-1}$), the liquidus temperature is approximately 1900 K higher [33, 34], requiring more energy to heat W to high homologous temperatures. Moreover, thermal and electrical conductivity of W are

higher than the ones of Fe [33, 34]. Considering these properties, first, less electric energy is dissipated into heat in W particles compared to in Fe particles. Secondly, heat in W particles is guided more effectively from contact zones into a greater volume, which causes a lower homologous temperature of W contact zones compared to Fe contact zones. The combination of higher strength and lower homologous temperature of the W particles eventually causes limited compression and diffusion of W, leaving greater residual porosity of W rich composites behind. The explanation is supported by cross section analyses. Exemplary micrographs, see Fig. 9, show that pores are

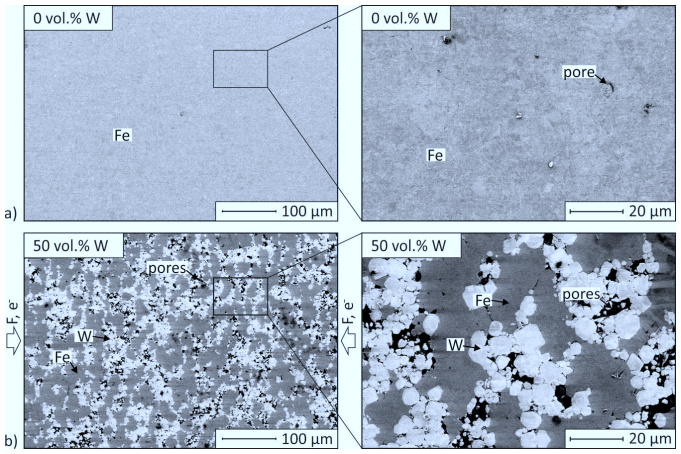

Figure 9: SEM cross sections of composites made from manually mixed coarse powders after consolidation at 80 kJ and 388 MPa. a) 0 vol.% W, b) 50 vol.% W.

predominantly present within W agglomerates, whereas large, homogeneous Fe volumes show good consolidation of former Fe particles. Given the previous results, manual mixing of Fe/W powders and subsequent consolidation by EDS was abandoned. The material-selective consolidation necessitates better intermixing of the constituents before EDS, which is possible by incomplete mechanical alloying.

3.2.2. Composites from energetically mixed fine powders

Composites made from energetically mixed fine powders were manufactured as graded samples and as homogeneous samples. The microstructure of each sublayer within the graded composites and the microstructure of the respective homogeneous samples are very similar (cf. Figs. 11 and 18). Hence, detailed characterisation of the FGM properties was carried out using homogeneous composites.

Microstructure. Microstructural characterisation of composites made from four different energetically mixed fine powders was carried out using SEM images, quantitative image analysis, and physical density measurements. Composites containing 25, 50 and 75 vol.% W made from powders mixed for 8 hours, and composites containing 75 vol.% W made from powder mixed for 4 hours were characterised. Fig. 10 shows the residual porosity of homogeneous composites as a function of W fraction, measured via quantitative image analysis and via Archimedes principle. Results of both measurement techniques agree with respect to the depicted error bars. Corresponding microstructures are shown in Fig. 11. Based on the porosity measurements of coarse powders, only the maximum discharge energy, 80 kJ, was applied for EDS with energetically mixed powders. Uniaxial pressure was set to 282 and 388 MPa. For completeness, the porosity of samples made from pure, coarse Fe powder was included in Fig. 10 although no energetic mixing was applied.

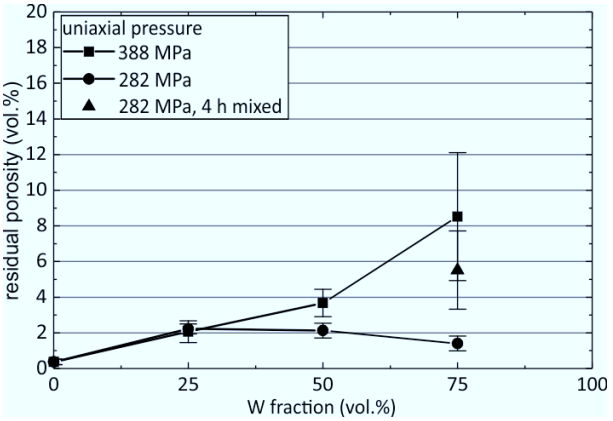

Figure 10: Residual porosity of composites made from energetically mixed Fe/W powders according to quantitative image analysis and the Archimedes principle. The discharge energy was set to 80 kJ, the uniaxial pressure to 282 and 388 MPa.

Consolidating energetically mixed powders with the same EDS parameters (80 kJ, 388 MPa) as previously used for manually mixed coarse powders, the porosity behaves qualitatively comparable with increasing W fraction. With the greatest porosity still being present in samples containing 75 vol.% W, the finer distribution of constituents after incomplete mechanical alloying causes a decrease of the maximum porosity from 20 to 8.5 vol.% compared to composites made from coarse powders. With less W, the impact of energetic mixing is still significant, but results in 10 vol.% lower porosity in 50 vol.% W composites and in 3 vol.% lower porosity in 25 vol.% W composites compared to composites made from coarse powders. These results correlate with the previous observation that the applied energetic mixing is more effective using powders of ≥50 vol.% W. Micrographs, see Fig. 11, reveal that pores in composites made from energetically mixed powders are primarily present between W volumes, as was observed for composites made from coarse powders, too. Since no W agglomerates exist after energetic mixing any more, the amount and size of pores in the corresponding composites is significantly decreased compared to composites made from coarse powders. Better constituents homogeneity hence allows the improvement of consolidation to an extent that former powder particle contact zones are unrecognisable. Overall, preferential orientation of constituents does not exist. The given observations apply to composites consolidated at 282 MPa, too. The corresponding porosities are also shown in Fig. 10. Using the lower uniaxial pressure, further decrease of the porosity to ≤2 vol.% is possible. The previously described porosity increase as a function of W fraction is replaced by a nearly constant porosity, that is much lower, with increasing W.

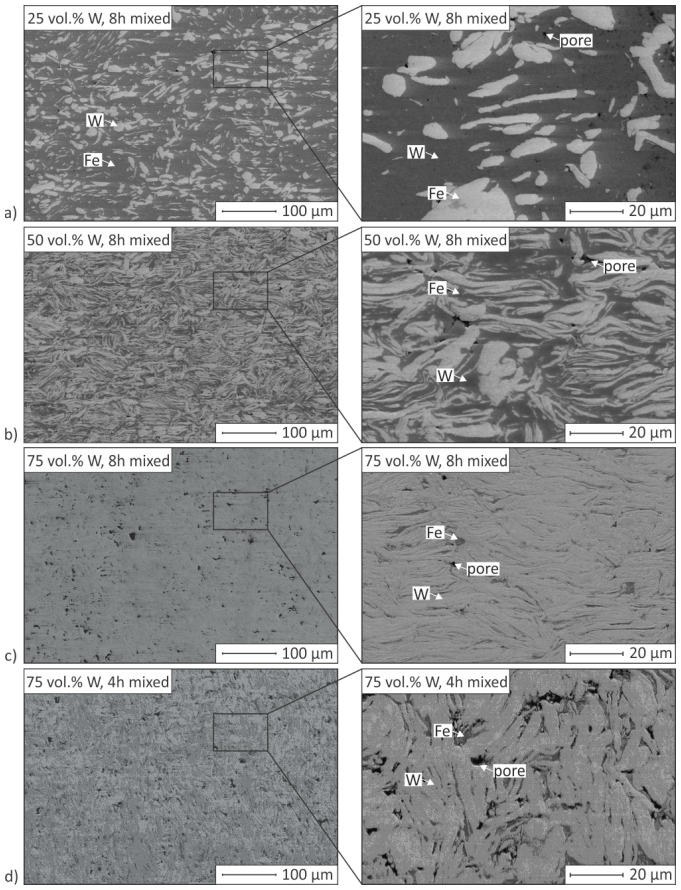

Figure 11: SEM images of Fe/W composites made from energetically mixed powders. a) 25 vol.% W, b) 50 vol.% W, c) 75 vol.% W, d) 75 vol.% W, mixed for 4 h only.

Three mechanisms, associated with energetic mixing, are assumed to generally improve the consolidation of Fe/W powders. First, after mixing, no W agglomerates, containing large pores, are present within the powders, potentially increasing the powder density even before EDS. Secondly, the powder is assumed to reach a higher and more homogeneously distributed temperature, particularly within W volumes. Electric energy in manually mixed coarse powders is dissipated primarily in Fe contact zones, which are separated from W volumes. This causes a material-selective increase of the homologous temperature. In contrast, energetically mixed powders exhibit large, direct Fe-W interfaces, causing better heat flow into W volumes and potentially greater energy dissipation, as phonons are scattered not only at contact zones, but also at phase boundaries [35]. Lastly, the homogeneously distributed Fe lamellae may cause a consolidation effect, similar to the principle of Supersolidus Liquid Phase Sintering (SLPS). In SLPS, prealloyed (steel) powder particles contain a low-melting eutectic network [36]. Upon heating, melting of the eutectic causes disintegration of particles, fast rearrangement of fragments and consolidation of the fill. While actual melting of Fe in Fe/W powders cannot be proven, strong softening may also cause W lamellae to slip off and fragments to rearrange.

The effect of stronger consolidation of Fe/W powders with lower uniaxial pressure is assumed to follow less elastic deformation, accompanied by smaller particle contact zones and higher ohmic resistance. Eventually, this may cause a higher temperature in the powder fill and more effective consolidation.

Upon superposition of residual stresses from energetic mixing and thermal stresses from EDS, some of the very dense samples exhibit crack networks, particularly composites containing 75 vol.% W. Samples of greater porosity may release stresses via deformation of pore surfaces. Approaches to avoid cracks may be stress-relief annealing of powders before EDS or limiting residual stresses in the first place, e.g. by shorter mixing. Annealing may promote the precipitation of impurity phases, hence 75 vol.% W containing samples were mixed for 4 hours only. The porosity measurements document an increase of porosity to 5.5 vol.% but the samples remain crack-free. The microstructure of the sample is shown in Fig. 11 d).

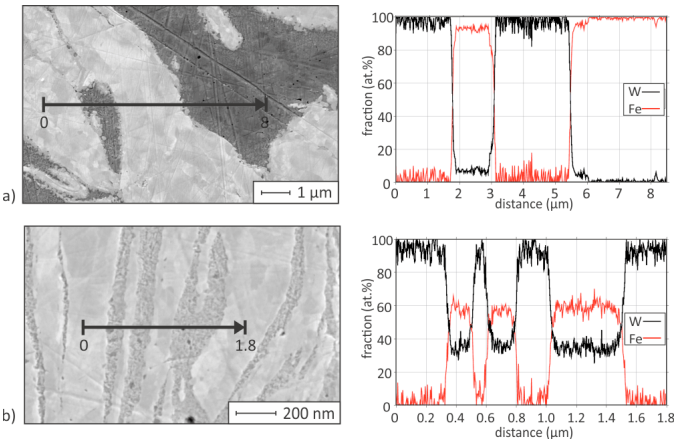

Figure 12: SEM cross sections of composites made from 8 hours long energetically mixed powders along with EDX line scans across Fe-W boundaries. The composites contain a) 50 vol.% W, b) 75 vol.% W. EDS parameters were set to 80 kJ and 388 MPa.

Selected composites were analysed via energy dispersive X-ray spectroscopy (EDX) and XRD to investigate constituent boundaries in detail. Fig. 12 contains SEM cross sections of composites made from powders energetically mixed for 8 hours and EDX line scans across microscopic Fe-W interfaces. In the 50 vol.% W composite, Fig. 12 a), the grey contrast and the corresponding EDX line scan reveal the existence of a very thin seam along the Fe-W interface. Considering its atomic stoichiometry the seam is suggested to represent the $Fe_{0.95}W_{0.05}$ solid solution, having formed by diffusion of W into Fe volumes during EDS. The composite containing 75 vol.% W, shown in Fig. 12 b), contains thinner lamellae. In accordance with previous assumptions that energetically mixed powders experience higher and more homogeneous temperatures during EDS with higher W fractions, the diffusion of W into Fe is enhanced. Pure iron volumes are replaced by a mixture of 60 at.% Fe and 40 at.% W, which may represent a mixed nanostructure of the $Fe_{0.95}W_{0.05}$ solid solution and the Fe_7W_6 intermetallic phase. Existence of these phases is confirmed by X-ray diffractograms, shown in Fig. 13.

In Fig. 13 diffractograms of powders before EDS and of

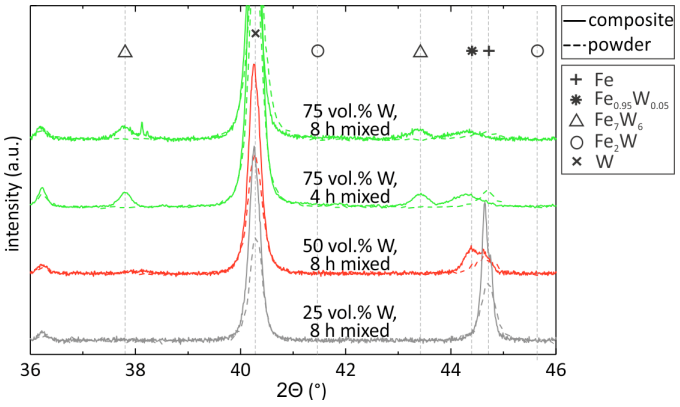

Figure 13: Diffractorgrams of energetically mixed powders and corresponding composites before and after EDS. Mixing was done for 4 and 8 hours, EDS parameters were set to as indicated.

composites after EDS are compared. Composites containing 25 vol.% W solely contain Fe and W both before and after EDS. EDS causes a slight shift of the 44.7° Fe peak towards the solid solution peak, which indicates limited diffusion of W into Fe volumes. In contrast, composites of higher W fractions show the EDS-induced development of new phases. In samples containing 50 vol.% W, EDX and XRD identify the $Fe_{0.95}W_{0.05}$ solid solution, composites of 75 vol.% W additionally contain the Fe_7W_6 intermetallic phase according to XRD. The formation of the intermetallic precipitate is insensitive to the mixing duration and to the uniaxial pressure during EDS with the selected parameters. At this stage, the goal of avoiding intermetallics in Fe/W composites can only be achieved with the current parameters for composites containing < 75 vol.% W. Further reducing the mixing duration, and thus minimising the constituent interface area, may help suppress interdiffusion and Fe_7W_6 precipitation.

Besides intermetallics, oxides may have detrimental effects on the performance of Fe/W composites used in the first wall. Fig. 6 compares the oxygen amount of used raw materials, energetically mixed powders and composites. Including incomplete mechanical alloying, after EDS, the oxygen concentration increases to approximately 1.5-fold of the natural O contamination. Taking a low natural concentration of ≤1.1 at.% into account, the final contamination is rather small, proving that an unregulated atmosphere during EDS is appropriate.

Thermo-physical properties. With an Fe/W FGM being part of the first wall, the FGM has to fulfil two crucial thermo-physical functions. First, thermally-induced geometric mismatches are to be balanced, secondly, heat has to be extracted from the reactor.

The first requirement can be achieved by converging the coefficient of thermal expansion of pure W and Eurofer via single sublayers of an Fe/W FGM. In the current work, the coefficient of thermal expansion of potential FGM sublayers was measured by dilatometry. Homogeneous composites of 0, 25, 50 and 75 vol.% W, consolidated at 80 kJ and 388 MPa after 8 hours energetic mixing of the powders, were tested. Since the available composite sizes were limited, small cubic samples of 5x4x2 mm^3 were extracted by electrical discharge machining (EDM). The sample surfaces were ground, polished and placed between two 10 mm long alumina rods. The set up achieves standard sample length of 25 mm and uses the temperature sensitivity of the dilatometer to full capacity. Prior to actual measurements, the setup was verified using small and regular scale pure W rods. Coefficients of thermal expansion of EDS composites that were calculated from dilatometry measurements are shown in Fig. 14.

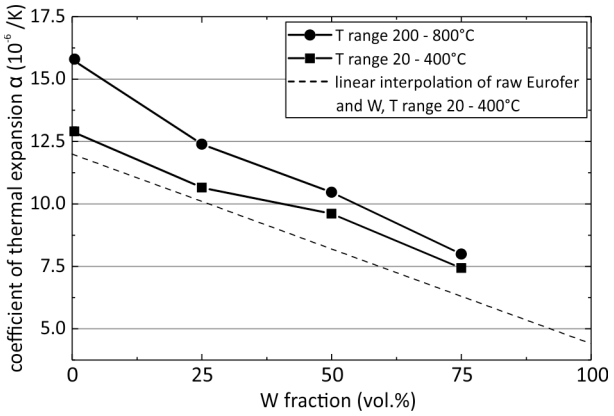

Figure 14: Coefficients of thermal expansion of homogeneous composites, given for two temperature ranges and linear interpolation of α literature data of pure Eurofer and pure W (dashed line) [33, 37].

Expansion coefficients regarding two temperature ranges are given in Fig. 14. The first set refers to a widely used temperature range for α measurements (20-400°C) and the second to a temperature range of interest for the current application (200-800°C). Comparing the data sets with linearly interpolated literature data of Eurofer and W expansion coefficients, a smooth convergence of measured expansion coefficients from pure Eurofer to pure W is visible across the FGM sublayers [33, 37]. In the temperature range 20-400°C, the coefficient of thermal expansion is slightly higher than expected, but still in good agreement with the linear interpolation. Data from the temperature range 200-800°C are further shifted due to the disproportionally strong volume increase at higher temperatures, well known for many metals. The data retain linear behaviour with increasing W fraction, indicating that EDS FGMs are capable of redistributing thermally-induced macro stresses.

Thermal conductivity λ is calculated as the product of density, heat capacity, and thermal diffusivity. These properties were measured using Archimedes principle at room temperature (RT), differential scanning calorimetry (DSC), and laser flash analysis (LFA), respectively. Results of the thermal conductivity as a function of the temperature and of the W fraction are shown in Fig. 15. At the lowest test temperature shown in Fig. 15 a), 200°C, the maximum thermal conductivity reaches one third of the conductivity of pure W (149 $W\,m^{-1}\,K^{-1}$ [37]). As for most metals, the thermal conductivity of the tested composites decreases with higher temperatures. Even though the Fe/W ratios of all composites containing ≤50 vol.% W differ strongly, λ only spans over a narrow range at all test temperatures. In contrast the 75 vol.% W composite con-

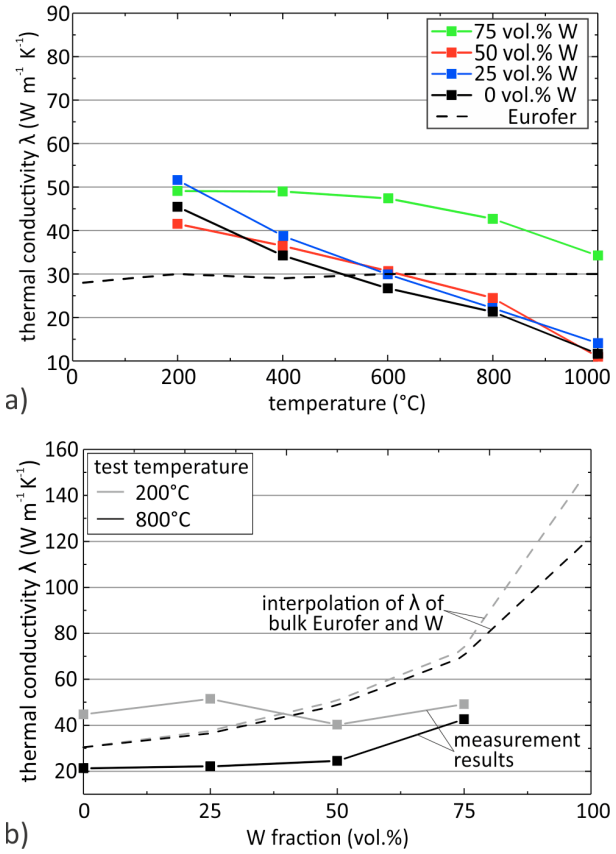

Figure 15: Thermal conductivity of Fe/W composites for different temperatures (a) and W fractions (b).

ducts heat much better, particularly at elevated temperatures. Different interacting effects cause the behaviours. A generally low thermal conductivity may be explained by the observed constituent interfaces, pores and impurity phases, all of which scatter phonons [35]. At 200°C, these effects, along with the observed $Fe_{0.95}W_{0.05}$ solid solution, cause composites containing 50 vol.% W to exhibit the lowest thermal conductivity. The solid solution and intermetallics are also present in 75 vol.% W composites, but the negative impact on λ is compensated by a higher W fraction. A W network throughout the composite that keeps the thermal conductivity high at elevated temperatures could not be observed in the context of microstructure analysis.

The thermal conductivity as a function of W fraction at 200 and 800°C, together with interpolated values of pure W and Eurofer, are shown in Fig. 15 b). As heat has to pass through Fe and W volumes successively in the characterised composites, the most conservative interpolation model, named the parallel model [38], is applied here to add the expected thermal conductivity behaviour of Eurofer/W FGMs as a function of W fraction. At 200°C the measured thermal conductivity behaviour versus the W fraction differs strongly from the interpolation model. Composites containing < 50 vol.% W exhibit higher conductivities compared to the model because pure Fe, used for fabrication, conducts heat better than Eurofer, used for the model. With higher W fractions, this effect loses impact, causing the measured data to be lower than the interpolation. At 800°C, the thermal conductivity is lower compared to the conductivity at 200°C, as previously described. A slight increase of the thermal conductivity with increasing W fraction can be observed, which is yet smaller than the conservative model suggests. From 200 to 800°C the thermal diffusivity of Fe is decreased further than the diffusivity of W [33, 37], causing the slight increase at higher W fraction amounts. The behaviour may additionally be explained by the diffusivity of pure metals generally being more sensitive to heat than the diffusivity of imperfect crystals, e.g solid solutions, which is more pronounced in composites of high W fractions.

Regarding the applicability of Fe/W FGMs in the first wall, it may be noted that up to 600°C, which is 50 K above the tolerable temperature of Eurofer, the thermal conductivity of the sublayers is higher than or equal to the conductivity of Eurofer. In current blanket designs, Eurofer represents the first wall's "bottle neck" for heat removal. Given this, the heat removal ability of an Fe/W FGM featured first wall is welcomed.

Mechanical properties. Besides meeting thermo-physical requirements, an Fe/W FGM has to be capable of conserving the structural integrity of the first wall. This is particularly important because it remains open whether the FGM will have to be an additional part in the first wall or whether it will replace fractions of the W and/or the Eurofer volumes. The latter option is preferable in terms of heat removal but transfers load bearing duties from the structural Eurofer part to the functional interlayer. W cannot be replaced because its minimum thickness is defined by plasma erosion losses.

To measure mechanical properties, four point bending tests, following a procedure suggested by Antusch et al. [39], were carried out. Homogeneous, (1x1x12) mm^3 samples were tested between RT and 300°C in air. Higher temperatures could not be applied due to limitations of the machine set up and sample oxidation. The supports were 1 mm in diameter. The lower supports were 10 mm apart, the upper ones 5 mm. Before actual measurements, the feasibility of the set up was verified applying FEA and using bulk W and steel samples. Stress-strain curves were calculated, utilising the standard four-point bending test formulae given in ASTM D7264 [40]. From these curves, Young's moduli, yield strengths, and maximum bending strengths were calculated. As the used formulae are technically only valid in the elastic regime, values of the maximum bending strength and of the maximum plastic strain have to be read with care. The results are shown as a function of W fraction in Fig. 16. Qualitatively, the increasing trends for all data sets (Young's modulus, yield strength, max bending strength) are in accordance with the linear interpolation of each property, calculated from the RT data of pure W and Eurofer [33, 37]. Regarding Young's moduli, measured data of composites containing ≤50 vol.% W are clearly lower than the linear interpolation. This is primarily because the composites contain soft Fe instead of martensitic Eurofer, the latter being considered for the interpolation. Young's moduli of Fe (196 GPa [34]) and Eurofer (220 GPa [33]) differ by approximately 24 GPa. Moreover, the measured values may be low due to micro-plastic deformation. The effect is well documented to occur in front of spheroidal

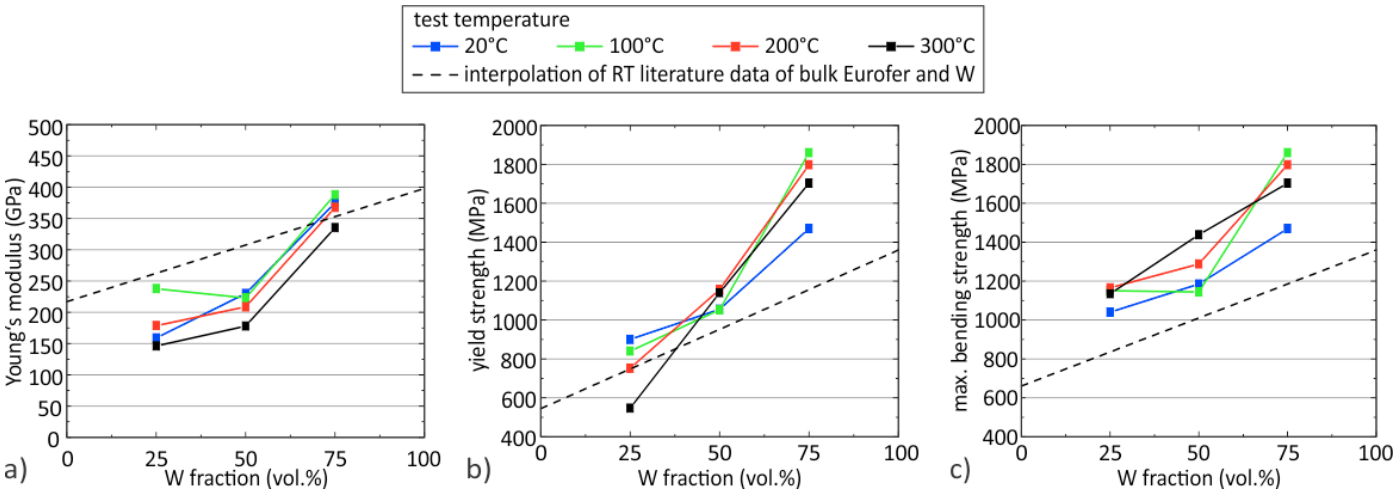

Figure 16: Mechanical properties of homogeneous Fe/W composites as a function of W fraction based on four-point bending measurements between room temperature (RT) and 300°C. a) Young's modulus, b) yield strength, c) max bending strength. Corresponding data, linearly interpolated from RT properties of pure W and pure Eurofer, are added as dashed lines.

graphite precipitates in cast iron, lowering the homogenised Young's modulus [41, 42]. Micro-plastic deformation may also occur around W particles in the composites. In composites containing 50 vol.% W, pores additionally lower Young's modulus. Both effects compensate an increase of Young's modulus, which would be expected due to the higher W fraction. Composites of 75 vol.% W show a high modulus because the soft Fe is replaced by the described $Fe_{0.95}W_{0.05}$+Fe_7W_6 nanostructure. Both of these impurity phases exhibit higher moduli than pure Fe. Except for the 25 vol.% W composite tested at RT, higher temperatures cause a decrease of Young's moduli of all composites. Considering all Fe/W ratios, Young's moduli decrease by about 50 GPa from RT to 300°C.

Yield strength and ultimate bending strength of all Fe/W ratios at RT are 100 to 200 MPa higher than the linear interpolation of pure W and Eurofer RT strengths. High strengths are retained at elevated temperatures. No clear temperature-dependent shift of the trends can be observed. Only the yield strength of composites containing 25 vol.% W decreases from 900 MPa at RT to 550 MPa at 300°C. Despite this drop, these composites are still stronger than Eurofer, which exhibits approximately 546 MPa and 465 MPa yield strength at RT and 300°C, respectively [33]. As the comparison of yield strength and ultimate bending strength reveals, composites of 25 vol.% W show distinct hardening above the yield stress, accompanied by plastic deformation. In contrast, this effect is strongly limited in composites containing ≥50 vol.% W. Table 2 gives the calculated plastic strain of the samples' outer fibres at rupture at all test temperatures.

The substantial difference in plastic deformation between composites containing 25 and ≥50 vol.% W is related to the increasing amount of W, which is brittle at the test temperatures. Moreover, the pronounced hardening during incomplete mechanical alloying of ≥50 vol.% W powders, and Fe volumes partially being replaced by intermetallics and the solid solution phases embrittle these composites. While pure Fe volumes are ductile, the solid solution and intermetallics prevent plastic deformation and increase the composite strength. The effects may also be observed at fracture surfaces.

Table 2: Plastic strain of the outer fibre at rupture in %, calculated from stress-strain curves, given for all tested combinations of Fe/W ratio and test temperature.

W fraction (vol.%)	RT	100°C	200°C	300°C
25	0.3	0.27	1.0	2.5
50	0.1	0.1	0.15	0.25
75	0	0	0	0

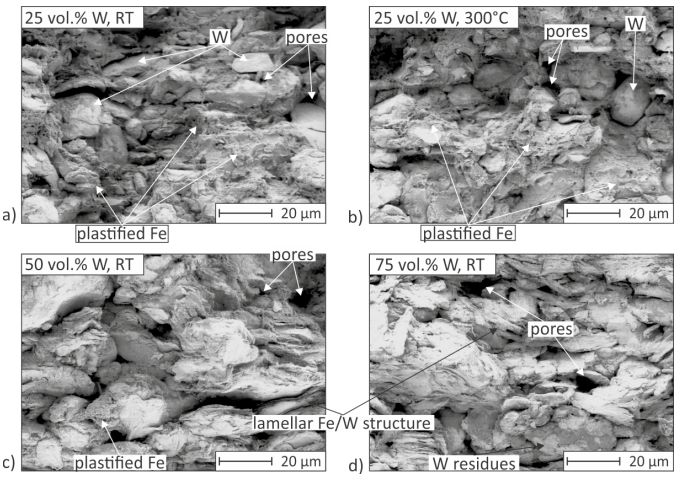

Figure 17: Fractography of four-point bending samples of different W fractions and test temperatures. a) 25 vol.% W, RT b) 25 vol.% W, 300°C, c) 50 vol.% W, RT, d) 75 vol.% W, RT.

Exemplary fractographic images of composites of different Fe/W ratios, tested at RT and 300°C, are shown in Fig. 17. The distinct plasticity of composites containing 25 vol.% W is readily observed in fracture areas. Deformed iron is represented in

Fig. 17 a) and b) by large irregularly shaped surfaces. These are a good indicator of ductile fracture. Smooth surfaces within the images correspond to disconnected, weak W bonds. On fracture surfaces of composites tested at 300°C, Fe volumes are more highly deformed compared to those in samples tested at RT. Composites of higher W fraction show no temperature related differences of fracture surfaces. Hence, only the fracture surfaces of samples that were tested at RT are shown in Fig. 17 c) and d). Almost no plastically deformed Fe volumes are visible in the images. Whether fracture occurred interparticularly or transparticularly remains open. Further analyses regarding the Fe-W interface qualities have to be carried out to in order to specify the failure mode.

3.2.3. Graded composites from energetically mixed fine powders and in-situ bonding to bulk pieces

Fusion relevant FGMs for the first wall will be consolidated in one step rather than in multiple steps. Fig. 18 shows regions of the cross section of a 2 mm thick Fe/W FGM made by EDS.

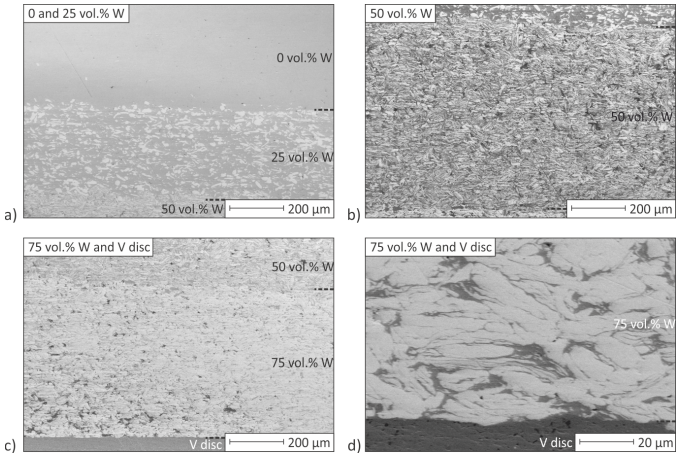

Figure 18: Microstructure of an Fe/W FGM, containing four sublayers, fabricated by EDS. a) 0 and 25 vol.% W, b) 50 vol.% W, c) 75 vol.% W and V disc, d) again 75 vol.% W and V disc higher magnified.

Powder containing 75 vol.% W, mixed for 4 hours, was filled into the EDS die, followed by powders containing 50 and 25 vol.% W, each mixed for 8 hours. Eventually, the coarse Fe powder was filled into the die. Masses of each powder were adjusted so that complete consolidation yields 0.25 mm (25 vol.% W), 0.5 mm (50 and 75 vol.% W) and 0.75 mm (0 vol.% W) thick sublayers. The powder stack was consolidated within a single discharge at 80 kJ and 388 MPa. Comparing the overview micrographs of the sublayers, Fig. 18, and the micrographs of corresponding homogeneous composites, Fig. 11, no distinct differences are visible. The bond zones of adjacent sublayers do not exhibit more defects than other locations of the microstructure. The similarity proves that the use of homogeneous composites for FGM properties testing is adequate.

The FGM comprises a thicker Fe layer compared to the other sublayers to account for the incomplete consolidation of the uppermost 0.3 mm of each sample. At the lowermost sublayer, increasing the thickness was avoided because the FGM was bonded to a counter piece. Sintering of the powder to polished 1 and 3 mm thick bulk W discs was unsuccessful at this stage, probably owing to the high electric and thermal conductivity of bulk W along with its high strength. In contrast, sintering to a polished 1 mm thick vanadium disk worked well, as can be seen from Fig. 18 d). The auxiliary V layer may help to bond the FGM to bulk W in a subsequent step. V-W joints were already successively fabricated by Basuki et al., applying hot pressing at 700°C [13]. Apart from that, the in-situ bonding of FGMs to bulk W will be further investigated. Bonding of the lowermost sublayer to bulk W may be enhanced by altering the bulk W surface prior to EDS. Reiser et al. have shown that depositing W by physical vapour deposition onto bulk W improves hot pressing [43]. This approach may work with EDS, too.

4. Summary

The current work presents a novel technique to manufacture Fe/W FGMs for the first wall of fusion reactors and characterises the FGM in detail. Obtained results can be assigned to four groups, namely powder processing, consolidation, composite properties, and in-situ bonding to bulk material.

- Powder processing
  - Energetic mixing, using a planetary mill with a ball-to-powder ratio of 5/1, rotation speed of at least 200 rpm and mixing durations of >2 h is reasonable to make Fe/W powders that contain distinct Fe and W volumes within each particle. An adequately fine distribution of the constituents is achieved after 4 and 8 hours mixing while no impurity phases (solid solution or intermetallics) form.
  - The energetic mixing is more efficient with higher W fractions, suggesting shorter mixing durations of W rich powders. Otherwise, high residual stresses and many constituent interfaces are generated.
- Powder consolidation via electro discharge sintering (EDS)
  - EDS is a promising technique to manufacture (graded) Fe/W composites. Samples are small, but up-scaling of EDS is possible, similar to SPS. Without up-scaling, approximately 4.5×10^6 EDS pieces of hexagonal base area are required to cover the first wall of DEMO with a honeycomb structure. Taking process time and the possibility of parallelisation into account, the high number is manageable.
  - Consolidation of manually mixed Fe/W powders produces composites of high porosity, particularly when the W fraction is high. In contrast, composites made from energetically mixed Fe/W powders consolidate well and with less porosity.
  - EDS yields lower residual porosity with higher discharge energy. The maximum available energy of 80 kJ (400 kA, 50 V) is suggested for FGM fabrication.

  - Most composites in this work were fabricated at 388 MPa uniaxial pressure. However, results indicate that lower pressures may be beneficial for improving consolidation and reducing residual residual porosity below 2 vol.%.

- Composite properties
  - Microstructural characterisation of Fe/W composites, made from energetically mixed powders, shows little porosity and fine distribution of Fe and W volumes.
  - While no impurity phases exist in the Fe/W powder, composites containing 50 vol.% W exhibit minor volumes of the solid solution $Fe_{0.95}W_{0.05}$ and composites containing 75 vol.% W additionally contain the intermetallic phase Fe_7W_6. These phases are expected to be reduced by optimizing mixing parameters and, thus, increasing the distinct constituent volumes in the powders prior to sintering.
  - With increasing W fraction, the Fe/W composites show a linear decrease of the coefficient of thermal expansion, proving applicability to redistribute thermally-induced macro stresses.
  - The expected increase of thermal conductivity with increasing W fraction of Fe/W composites is less pronounced than the most conservative parallel model predicts. This is owing to pores, interfaces, and impurity phases not being taken into account by the parallel model. Albeit the named defects, thermal conductivity of all composites is higher than or equal to the conductivity of Eurofer, which is the bottle neck in terms of removing heat from the reactor core.
  - The mechanical parameters Young's Modulus, yield strength, and ultimate bending strength of Fe/W composites reveal an increase with increasing W fraction. While Young's modulus is somewhat lower than a linear interpolation model predicts, yield strength and bending strength of all samples are higher than linear interpolations predict.

- In-situ bonding to bulk material
  - In-situ bonding of FGMs to bulk W discs was unsuccessful at this stage. In contrast, in-situ bonding to V discs succeeded.

Appendix A. Acknowledgements

This work has been carried out within the framework of the EUROfusion Consortium and has received funding from the Euratom research and training programme 2014-2018 under grant agreement No 633053. The views and opinions expressed herein do not necessarily reflect those of the European Commission.

Appendix B. References

[1] J. W. Coenen, S. Antusch, M. Aumann, W. Biel, J. Du, J. Engels, S. Heuer, A. Houben, T. Hoeschen, B. Jasper, F. Koch, J. Linke, A. Litnovsky, Y. Mao, R. Neu, G. Pintsuk, J. Riesch, M. Rasinski, J. Reiser, M. Rieth, A. Terra, B. Unterberg, T. Weber, T. Wegener, J.-H. You, C. Linsmeier, Materials for DEMO and reactor applications - boundary conditions and new concepts, Physica Scripta T167 (2016) 1–11.

[2] V. Philipps, Tungsten as material for plasma-facing components in fusion devices, Journal of Nuclear Materials 415 (2011) S2–S9.

[3] T. Weber, J. Aktaa, Numerical assessment of functionally graded tungsten/steel joints for divertor applications, Fusion Engineering and Design 86 (2011) 220–226.

[4] Y. Igitkhanov, B. Bazylev, R. Fetzer, The quantification of the key physics parameters for the DEMO fusion power reactor and analysis of the reactor relevant physics issues, KIT Scientific Publishing, 2014.

[5] D. Qu, W. W. Basuki, J. Aktaa, Numerical assessment of functionally graded tungsten/Eurofer coating system for first wall applications, Fusion Engineering and Design 98-99 (2015) 1389–1393.

[6] Y. Igitkhanov, R. Fetzer, B. Bazylev, Effect of design geometry of the DEMO first wall on the plasma heat load, Nuclear Materials and Energy 9 (2016) 560–564.

[7] S. Heuer, T. Weber, G. Pintsuk, J. Coenen, J. Matějíček, C. Linsmeier, Aiming at understanding thermo-mechanical loads in the first wall of DEMO: Stress–strain evolution in a eurofer-tungsten test component featuring a functionally graded interlayer, Fusion Engineering and Design 135 (2018) 141–153.

[8] T. Weber, M. Stüber, S. Ulrich, R. Vaßen, W. W. Basuki, J. Lohmiller, W. Sittel, J. Aktaa, Functionally graded vacuum plasma sprayed and magnetron sputtered tungsten/Eurofer97 interlayers for joints in helium-cooled divertor components, Journal of Nuclear Materials 436 (2013) 29–39.

[9] D. Qu, W. W. Basuki, J. Gibmeier, R. Vaßen, J. Aktaa, Development of functionally graded tungsten/Eurofer coating systems for first wall applications, Fusion Science and Technology 68 (2015) 578–581.

[10] D. Qu, Z. Zhou, J. Tan, J. Aktaa, Characterization of W/Fe functionally graded materials manufactured by resistance sintering under ultra-high pressure, Fusion Engineering and Design 91 (2015) 21–24.

[11] W. W. Basuki, J. Aktaa, Diffusion bonding between W and Eurofer97 using V interlayer, Journal of Nuclear Materials 429 (2012) 335–343.

[12] W. W. Basuki, R. Dahm, J. Aktaa, Thermomechanical analysis of diffusion-bonded tungsten/Eurofer97 with a vanadium interlayer, Journal of Nuclear Materials 435 (2014) 635–639.

[13] W. W. Basuki, J. Aktaa, Process optimization for diffusion bonding of tungsten with Eurofer97 using a vanadium interlayer, Journal of Nuclear Materials 459 (2015) 217–234.

[14] H. Noto, A. Kimura, H. Kurishita, S. Matsuo, S. Nogami, Evaluation of feasibility of tungsten/oxide dispersion strengthened steel bonding with vanadium insert, Materials Transactions 54 (2013) 451–455.

[15] Z. Zhong, H.-C. Jung, T. Hinoki, A. Kohyama, Effect of joining temperature on the microstructure and strength of tungsten/ferritic steel joints diffusion bonded with a nickel interlayer, Journal of Materials Processing Technology 210 (2010) 1805–1810.

[16] G. Zou, J. Yang, A. Wu, G. Huang, D. Zhang, J. Ren, Q. Wang, Diffusion bonding of tungsten to copper and its alloy with Ti foil and Ti/Ni/Ti multiple interlayers, Journal of Materials Science and Technology 19 (2003) 189–192.

[17] Y.-I. Jung, J.-Y. Park, B.-K. Choi, D.-W. Lee, S. Cho, Interfacial microstructures of HIP joined W and ferritic–martensitic steel with Ti interlayers, Fusion Engineering and Design 88 (2013) 2457–2460.

[18] J.-Y. Park, Y.-I. Jung, B.-K. Choi, D.-W. Lee, S. Cho, Joining of tungsten to ferritic/martensitic steels by hot isostatic pressing, Journal of Nuclear Materials 442 (2013) 541–545.

[19] J.-C. Wang, W. Wang, R. Wei, X. Wang, Z. Sun, C. Xie, Q. Li, G.-N. Luo, Effect of Ti interlayer on the bonding quality of W and steel HIP joint, Journal of Nuclear Materials 485 (2017) 8–14.

[20] W. S. Liu, Q. S. Cai, Y. Z. Ma, Y. Y. Wang, H. Y. Liu, D. X. Li, Microstructure and mechanical properties of diffusion bonded W/steel joint using V/Ni composite interlayer, Materials Characterization 86 (2013) 212–220.

[21] J. Li, X. Fang, J. F. Yang, G.-J. Qiao, Influence of different interlayers

metals on properties of diffusion bonding joint of tungsten to copper, Materials Science Forum 620-622 (2009) 65–68.
[22] Q. Cai, W. Liu, Y. Ma, H. Liu, Microstructure, residual stresses and mechanical properties of diffusion bonded tungsten–steel joint using a V/Cu composite barrier interlayer, International Journal of Refractory Metals & Hard Materials 48 (2015) 312–317.
[23] T. Chehtov, J. Aktaa, O. Kraft, Mechanical characterization and modeling of brazed Eurofer-tungsten-joints, Journal of Nuclear Materials 367-370 (2007) 1228–1232.
[24] B. A. Kalin, V. T. Fedotov, O. N. Sevrjukov, A. Moeslang, M. Rohde, Development of rapidly quenched brazing foils to join tungsten alloys with ferritic steel, Journal of Nuclear Materials 329-333 (2004) 1544–1548.
[25] B. A. Kalin, V. T. Fedotov, O. N. Sevrjukov, A. N. Kalashnikov, A. N. Suchkov, A. Moeslang, M. Rohde, Development of brazing foils to join monocrystalline tungsten alloys with ODS-Eurofer steel, Journal of Nuclear Materials 367-370 (2007) 1218–1222.
[26] Y. Ma, Q. Cai, W. Liu, S. Liu, Microstructure and mechanical properties of brazed tungsten/steel joint for divertor applications, Materials Science Forum 789 (2014) 384–390.
[27] Y. Nishi, Y. Mogi, K. Oguri, Preparation of Fe–W amorphous films by an electroplating method, Journal of Materials Science Letters 14 (1995) 1–3.
[28] N. Tsyntsaru, J. Bobanova, X. Ye, H. Cesiulis, A. Dikusar, I. Prosycevas, J. P. Celis, Iron-tungsten alloys electrodeposited under direct current from citrate-ammonia plating baths, Surface and Coatings Technology 203 (2009) 3136–3141.
[29] Z. Zhou, S. Guo, S. Song, W. Yao, C. Ge, The development and prospect of fabrication of W based plasma facing component by atmospheric plasma spraying, Fusion Engineering and Design 86 (2011) 1625–1629.
[30] T. Weber, Development and optimization of graded tungsten/eurofer97 joints for divertor components (original title: Entwicklung und Optimierung von gradierten Wolfram/Eurofer97-Verbindungen für Divertorkomponenten), Ph.D. thesis, Karlsruher Institut für Technologie (2012).
[31] P. Schütte, Aufbau einer Kurzzeitsinteranlage zur Herstellung verschleißbeständiger Verbundwerkstoffe, Ph.D. thesis, Ruhr-Universtität Bochum (2012).
[32] C. Suryanarayana, Mechanical Alloying and Milling, CRC Press, 2004.
[33] F. Tavassoli, Fusion demo interim design criteria (DISDC)/appendix A: Material design limit data/A3.S18E Eurofer steel, DMN/DIR/NT/2004-000/A, Tech. rep., DMN Technical Report (2004).
[34] H. Berns, W. Theisen, Eisenwerkstoffe - Stahl und Gusseisen, Springer, 2008.
[35] G. Gottstein, Physikalische Grundlagen der Materialkunde, 3rd Edition, Springer, 2007.
[36] R. M. German, Sintering Theory and Practice, John Wiley & Sons Inc, 1996.
[37] ITER Materials Properties Handbook (MPH), ITER Doc. G 74 MA 16 04-05-07 R0.1 (internal project document distributed to the ITER Participants), 2017.
[38] R. C. Progelhof, J. L. Throne, R. R. Ruetsch, Method for predicting the thermal conductivity of composite systems: A review, Polymer Engineering and Science 16 (1976) 615 – 625.
[39] S. Antusch, D. E. J. Armstrong, T. B. Britton, L. Commin, J. S. K.-L. Gibson, H. Greuner, J. Hoffmann, W. Knabl, G. Pintsuk, M. Rieth, S. G. Roberts, T. Weingaertner, Mechanical and microstructural investigations of tungsten and doped tungsten materials produced via powder injection molding, Nuclear Materials and Energy 1-2 (2015) 22–31.
[40] ASTM Subcommittee D30.04, Standard Test Method for Flexural Properties of Polymer Matrix Composite Materials (ASTM D7264), ASTM International, 2015.
[41] L.-Y. Fang, K. E. Metzloff, R. C. Voigt, C. R. Loper, Der Elastizitätsmodul von graphitischen Gußeisen und Nachdruck des Vortrags "young's modulus in graphitic cast irons." beim 61. Gießerei-Weltkongress, Beijing, ZVG.
[42] D. Lohe, O. Vöhringer, E. Macherauch, The influence of graphite shape on mechanical properties of ferritic cast iron, Mechanical behaviour of materials. Pergamon Press, 1983.
[43] J. Reiser, L. Garrison, H. Greuner, J. Hoffmann, T. Weingärtner, U. Jäntsch, M. Klimenkov, P. Franke, S. Bonk, C. Bonnekoh, S. Sickinger, S. Baumgärtner, D. Bolich, M. Hoffmann, R. Ziegler, J. Konrad, J. Hohe, A. Hoffmann, T. Mrotzek, M. Seiss, M. Rieth, A. Möslang, Ductilisation of tungsten (W): Tungsten laminated composites, International Journal of Refractory Metals & Hard Materials 69 (2017) 66–109.